Conrad D. James
e-mail: cdjame@sandia.gov

Murat Okandan
e-mail: mokanda@sandia.gov

Paul Galambos
e-mail: pcgalam@sandia.gov

Seethambal S. Mani
e-mail: ssmani@sandia.gov

Sandia National Laboratories,
P.O. Box 5800,
Albuquerque, NM 87185

Dawn Bennett
e-mail: dawnb@umbc.edu
The University of Maryland,
Baltimore County,
1000 Hilltop Circle,
Baltimore, MD 21250

Boris Khusid
e-mail: khusid@adm.njit.edu
New Jersey Institute of Technology,
University Heights,
Newark, NJ 07102

Andreas Acrivos
e-mail: acrivos@scisun.sci.ccny.cuny.edu
The Levich Institute,
The City College of New York,
140th Street & Convent Avenue,
New York, NY 10031

Surface Micromachined Dielectrophoretic Gates for the Front-End Device of a Biodetection System

We present a novel separation device for the front-end of a biodetection system to discriminate between biological and non-biological analytes captured in air samples. By combining AC dielectrophoresis along the flow streamlines and a field-induced phase-separation, the device utilizes "dielectrophoretic gating" to separate analytes suspended in a flowing fluid based on their intrinsic polarizability properties. The gates are integrated into batch fabricated self-sealed surface-micromachined fluid channels. We demonstrate that setting the gate to a moderate voltage in the radio frequency range removed bacteria cells from a mixture containing non-biological particles without the need for fluorescent labeling or antibody-antigen hybridization, and also validate experimentally basic relations for estimating the gate performance. [DOI: 10.1115/1.2136924]

Introduction

There is an increasing demand for novel systems to enable the rapid detection of biological materials in the field or their continuous monitoring in a hospital setting. The first step in the operation of such a system consists of concentrating and separating the analytes of interest from the background matrix and positioning them into selected locations for analysis. The next step is to provide a "trigger/cue" that signals the detection of a biological substance. Many biological detection systems use a trigger/cue based on ultraviolet laser-induced fluorescence (UV-LIF), which can detect biosignatures specific to living organisms, such as amino acids and coenzymes [1,2]. UV-LIF and other optical techniques are the gold standards for biological detection in the laboratory setting, but they suffer from several drawbacks. For instance, specificity is a major concern in that contaminants, such as engine exhaust particles, will also fluoresce under UV excitation, triggering high rates of false positives [2]. In addition, UV-LIF technology is difficult to miniaturize, a process that would reduce cost, increase portability, and facilitate the rapid detection in nonlaboratory settings. Optical systems require fragile components and delicate alignment of sources, samples, and detectors, making such systems more difficult to implement in small portable devices where vibrations and accelerations can compromise detector function. Gas phase lasers are commonly used as UV sources in such systems [3], but these lasers are bulky, draw large amounts of power, and lack the robustness necessary for typical field applications. Also, the high initial and lifetime maintenance cost of UV-LIF laser sources limits overall system affordability. Currently, solid-state lasers, which are compact, rugged, and use less power, are now being employed [4] and have been successfully demonstrated in the field [5], but specificity and sensitivity problems remain.

For these and other reasons, many researchers are pursuing nonoptical methods, such as dielectric spectroscopy and impedance monitoring, for biological characterization and detection [6,7]. The focus of the present work is a related technique, dielectrophoretic separation, which is being examined as a detection/separation method [8–10]. Compared to other available methods, AC dielectrophoresis (DEP) is particularly well suited for collecting and separating particles because the application of a high-frequency (megahertz) AC field suppresses undesirable electrode polarization, electrolytic effects, and electroconvection in the liquid. Also, the polarization forces exerted on analytes are insensitive to the particle charge, a property of analytes that is difficult to control. A hypothetical front-end of a biological detection system using "dielectrophoretic gates" [11] is shown in Fig. 1. After an air sampler collects a sample, the captured analytes are suspended

Contributed by the Fluids Engineering Division of ASME for publication in the JOURNAL OF FLUIDS ENGINEERING. Manuscript received July 20, 2004; final manuscript received April 21, 2005. Assoc. Editor: Dennis Siginer.

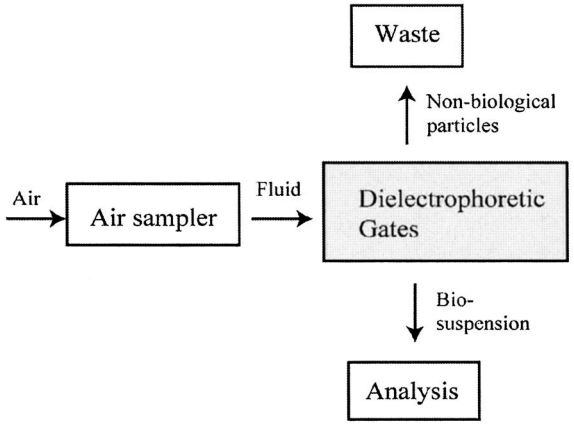

Fig. 1 Proposed biodetection system that uses dielectrophoretic gates as a trigger/cue to signal the detection of an unknown biological analyte, and to separate biological from non-biological materials

in a carrier fluid for transport to the dielectrophoretic gates. The gates are essentially sources of high-frequency AC voltage that will impart electrokinetic forces on the flowing analytes. The gate will separate biological (cellular) from nonbiological analytes using the frequency dependence of the analytes' complex dielectric permittivity, an intrinsic property of all substances. We showed [11] that, in addition to the dielectrophoretic force imparted by the gate along the flow streamlines, long-range electrical and hydrodynamic forces due to interparticle interactions lead to an accompanying phase separation of constituents, thus enhancing separation. After the cellular material is collected, the contaminants can be flushed as waste, and the remaining cellular material can be transported to the detector for identification. Specifically, we demonstrated the dielectrophoretic and field-induced phase separation of heat-killed bacteria and latex microspheres in a surface micromachined fluidic device [11].

The purpose of this paper is: (i) to describe a technique for the fabrication of a microchannel equipped with the dielectrophoretic gate and the experimental setup and procedures for studying the gate performance not included in Ref. [11] due to page constraints, (ii) to present new experimental data on the motion and separation of biological and nonbiological particles, and (iii) to validate a simplified method for evaluating the particle velocity flowing through the gate.

Dielectrophoretic Gate Theory

A new concept for the electroseparation of bioparticles from nonbiological materials, termed "dielectrophoretic gating," combines the field-induced DEP along the flow streamlines and phase transition for manipulating particles in microfluidics [11]. Figure 2(*a*) depicts the gate, which consists of a pair of microelectrodes that span a fluid channel, perpendicular to the direction of fluid flow. When an AC voltage is applied to the microelectrodes, an electric field is generated within the fluid channel. When exposed to such a spatially nonuniform electric field, a particle flowing through the channel will polarize and acquire a dipole moment that will interact with the electric field, generating a time-averaged dielectrophoretic force $\mathbf{F}_{\mathrm{DEP}}$, given by [12]

$$\mathbf{F}_{\mathrm{DEP}} = \tfrac{3}{2}\varepsilon_0\varepsilon_f V_p \,\mathrm{Re}[\beta^*(\omega)]\,\nabla\,\mathbf{E}^2_{\mathrm{rms}} \tag{1}$$

where ε_0 and ε_f are the vacuum and fluid permittivity, respectively, V_p is the particle volume, $\mathrm{Re}[\beta^*(\omega)]$ is the real component of the relative particle polarization $\beta^*(\omega)$ at the field frequency ω, and $\nabla\mathbf{E}^2_{\mathrm{rms}}$ is the gradient of the squared root-mean-square electric field. Under this force, the particle is either attracted toward

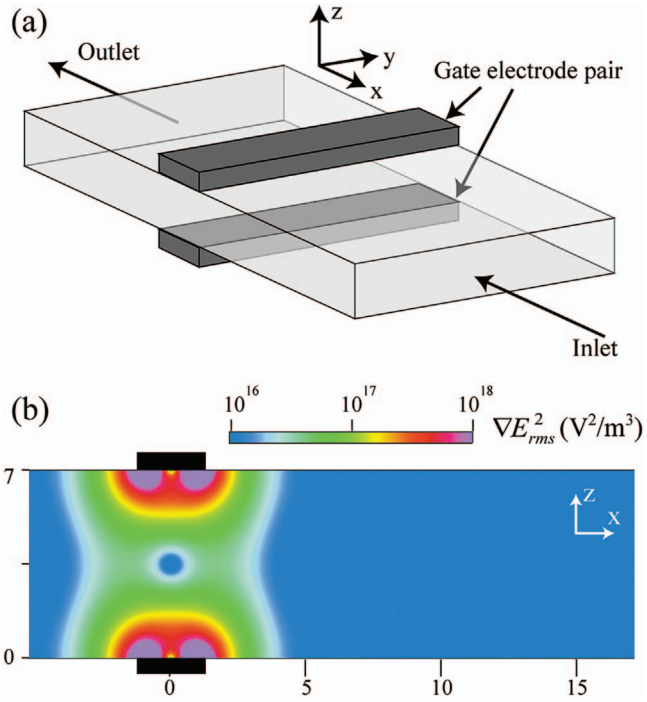

Fig. 2 (*a*) Schematic of a dielectrophoretic gate consisting of two electrodes arranged perpendicular to the fluid flow. (*b*) Log plot of the simulated $\nabla\mathbf{E}^2_{\mathrm{rms}}(x,z)$ for the two-electrode dielectrophoretic gate. Electrodes (black rectangles) are added for clarity. Dimensions are in μm.

[$\mathrm{Re}(\beta^*)>0$, positive DEP (pDEP)] or repelled from [$\mathrm{Re}(\beta^*)<0$, negative DEP (nDEP)] regions of large $\nabla\mathbf{E}^2_{\mathrm{rms}}$, depending on whether the particle is more or less polarizable than the liquid, respectively. We previously demonstrated for pDEP [13,14] and nDEP [15] that the predictions of a single-particle model, which considers the combined effect of $\mathbf{F}_{\mathrm{DEP}}$, the Stokes drag force, and the gravity force acting on a single particle are quantitatively consistent with experimental data on the particle motion. These predictions were made for suspensions with ~0.1% (v/v) polarized particles under the action of strong electric fields, even though $\beta^*(\omega)$ was measured at low fields (approximately, volts per millimeter). In the radio frequency range, the relative polarizability of a particle immersed in water is mainly influenced by the ratio of the capacitances of the particle and of the water, so that a reasonable estimate of $\mathrm{Re}(\beta^*)$ is given by

$$\mathrm{Re}(\beta^*) \approx \frac{\varepsilon_p - \varepsilon_f}{\varepsilon_p + 2\varepsilon_f} \tag{2}$$

where ε_p is the particle permittivity. The dielectric constant of water at radio frequencies is about 78. In contrast, the dielectric constants of soil components and common industrial and natural materials (for example, resins, plastics, carbon black, soot, ash, and gravel), when dry, fall in the range 1.5–15. Since the particle polarization in the radio frequency range is mainly specified by its bulk dielectric constant, these materials, when dispersed, in water will exhibit strong negative dielectrophoresis. In contrast, biological particles, such as cells, have polarizabilities typically close to or greater than that of water. Thus, we employ an AC field in the radio frequency range (0.1–30 MHz) to separate biological from nonbiological particles in our device. Another essential advantage of operating in this frequency range is that undesirable electric effects in water, such as electrolysis and other irreversible chemical reactions, electroosmosis, and electroconvection are suppressed, making this scheme particularly well suited for microfluidic applications. Since electrophoretic effects also vanish at

megahertz frequencies, this separation technique relies on the bulk polarization properties of a particle, given by $\mathrm{Re}(\beta^*)$, that are insensitive to the particle surface properties which may vary randomly due to environmental effects or intentionally due to the method of aerosolization.

The range of $\mathbf{F}_{\mathrm{DEP}}$ operating along the flow streamlines was extended throughout the height (z-axis) of the channel by placing an electrode on the top and bottom surfaces of the channel. This helps to increase the gating efficiency in that particles suspended in a fluid flowing at any position in the yz plane will be subjected to $\mathbf{F}_{\mathrm{DEP}}$. Figure 2($b$) shows a two-dimensional simulation of the dielectrophoretic gate (CFD-ACE+ Version 2003.0.136). The grid density was 10 points per micrometer, and the electrodes were set to 10 V. In this simulation, the height of the channel was 7 μm, and the electrode surfaces were 2 μm wide. The topography at the electrode edges was neglected, and all other surfaces were set to the boundary condition of zero-normal current. The field gradient is largest at close distances to the microelectrodes, and in this example, $\nabla\mathbf{E}^2_{\mathrm{rms}}$ maintains a value of $\sim 10^{17}\ \mathrm{V}^2/\mathrm{m}^3$ or greater throughout the z-axis near the gate. Upon injecting a solution of analytes that are more polarizable than the suspending fluid, the analytes will accelerate under pDEP toward the regions of highest $\nabla\mathbf{E}^2_{\mathrm{rms}}$, which is near the microelectrodes. Solving the equation of motion for a particle by taking into account $\mathbf{F}_{\mathrm{DEP}}$ and the drag force while neglecting the interparticle interactions and the gravity force, the velocity of a small spherical particle of radius a traveling in a flowing fluid is given by [13,16]

$$\mathbf{u} = \mathbf{v} + \frac{\mathbf{F}_{\mathrm{DEP}}}{6\pi\eta a}, \tag{3}$$

where η and $\mathbf{v}$ are the fluid viscosity and velocity, respectively. For large $\nabla\mathbf{E}^2_{\mathrm{rms}}$, $\mathbf{F}_{\mathrm{DEP}}$ will attract highly polarizable analytes to the microelectrodes where they will come to rest. In contrast, for analytes that are less polarizable than the fluid, $\mathbf{F}_{\mathrm{DEP}}$ will act as a repulsive force as the analytes seek to migrate toward regions of low $\nabla\mathbf{E}^2_{\mathrm{rms}}$. Thus, if the particles injected into the channel have low polarizability, they will be carried with the fluid flow until the value of $\nabla\mathbf{E}^2_{\mathrm{rms}}$ reaches the point at which the particles start being subjected to nDEP. This nDEP force will then decelerate the particles, producing a drag force as the particle motion begins to oppose the fluid motion, and at some location upstream from the gate, the particles will come to rest at the point where $\mathbf{F}_{\mathrm{DEP}}$ equals the drag force. A larger fluid velocity will push the particles closer to the gate, whereas a smaller fluid velocity will allow the particles to be repelled at greater distances from the gate. Upon injection of a mixture of low- and high-polarizability particles, the opposing nDEP and pDEP forces will separate the particles rapidly.

After coming to rest, the particles interact with one another due to their polarization. As the distance between the particles decreases, the polarization force increases, greatly exceeding the magnitude given by the dipole approximation for the interparticle separation smaller that the particle radius. When the local concentration of the accumulated particles exceeds a threshold value so that the average interparticle separation becomes sufficiently small, the polarization forces cause the particles to undergo a phase transition (referred to as the electrorheological effect [17]) and to form a distinct front between the regions enriched with and depleted of particles [11]. The evolution of the particle patterns formation is well described by a proposed electrohydrodynamic model [11,18], which does not require any fitting parameters. This three-dimensional model encompasses the quasi-steady electrodynamic equations coupled with the momentum and continuity balance equations of the "mixture" model for a suspension. Now we shall demonstrate that the simulation of the electric field configuration and Eqs. (1) and (3) provides a simplified method for estimating the particle velocity and the front location, which are needed for the design and optimization of the gate performance.

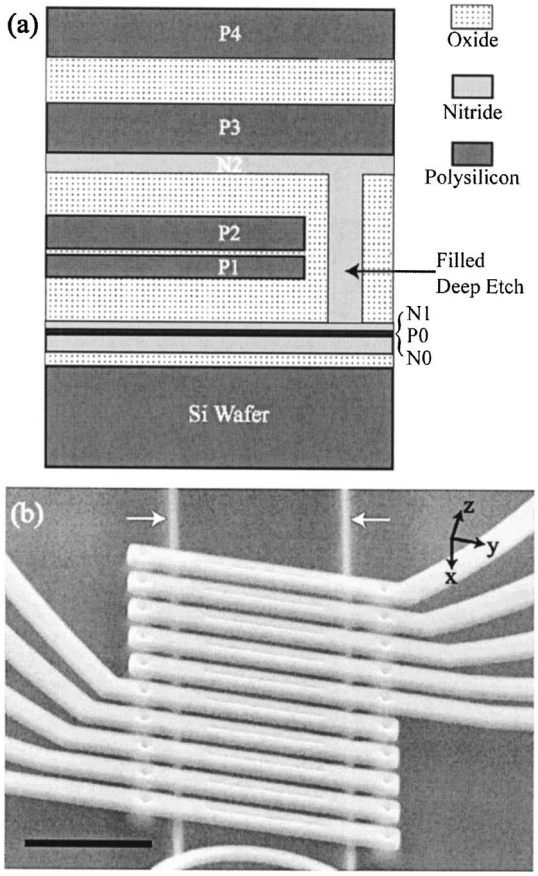

Fig. 3 (*a*) SwIFT™ film stack with five polysilicon, three silicon nitride, and four sacrificial silicon oxide layers. (*b*) Scanning electron micrograph of a series of dielectrophoretic gates. The fluid channel sidewalls are denoted by the white arrows. Scale bar=30 μm.

Device Fabrication

The devices were fabricated at the Sandia National Laboratories Microelectronics Development Laboratory. The dielectrophoretic gate we present here was fabricated using a previously described process termed SwIFT™ (surface micromachining with integrated fluidic technology) [19]. SwIFT is a sacrificial layer method that uses multiple layers of structural materials (polysilicon and silicon nitride) and sacrificial materials (silicon oxide) to build devices. The SwIFT process begins with a 6 in. bare (100) n-type wafer with 2–20 Ω cm resistivity (Fig. 3(a)). Next, the bulk silicon is isolated from the devices with a 0.6 μm layer of thermally grown silicon oxide followed by a 0.8 μm layer of nonstoichiometric (silicon-rich) low-stress silicon nitride (N0). Up to five layers of fine-grained doped polysilicon (P0–P4) are deposited from silane in a low-pressure chemical vapor-deposition furnace. These layers are used for making electrical connections and microelectrodes in order to impart electric fields into microfluidic compartments. Polysilicon layers are on the order of 1–2 μm thick, with the exception of P0, which is 0.3 μm. The sacrificial oxide layers are deposited using both low pressure chemical vapor deposition and plasma enhanced chemical vapor deposition. Chemical-mechanical polishing is used to reduce the topography in the final two sacrificial oxide layers. The structural layers of silicon nitride (N1: 0.3 μm, N2: 0.8 μm thick) provide optically transparent and electrically insulating surfaces that serve as barriers for the fluidic components. Figure 3(a) indicates a deep etch through several sacrificial oxide films down to N1. This trench is then filled with

N2, forming sidewalls and ceiling covers for fluidic channel components. The total film thickness is 16 μm, and the distance between N1 and N2 is $\sim$7 μm. The channels are fabricated in a fully encapsulated state, obviating the need for substrate bonding, a process that slows the device production and reduces reproducibility.

After completing the surface micromachining, access ports to the fluidic devices are fabricated using deep reactive ion etching [20]. The sacrificial oxide layers in devices are then removed in an HF-based etchant at 20°C for 100–200 min depending on the length of the fluidic channel. The devices are then rinsed in deionized (DI) water and dried in supercritical CO_2. Figure 3(*b*) shows a completed fluidic device with integrated dielectrophoretic gates. The N2 channel sidewalls are visible, along with the P3 electrode traces perpendicular to the fluid channel axis. P4 was not utilized in this particular device. The circular depressions are vias that connect the P3 microelectrodes to the P0 microelectrodes (not visible), allowing them to be held at the same potential. The long depressions in the center of the P3 traces are due to etches in N2 that allow the P3 microelectrode to be in direct contact with the fluid flowing through the channel. Similar etches are made in N1 to allow P0 to contact the fluid.

Experimental Methods

Following [11], experiments were performed on aqueous mixtures of latex beads (1 μm dia, Duke Scientific) chosen to be representative on non-biological particles and heat-killed Staphylococcus aureus bacteria (Molecular Probes) chosen as sample biological particles. Latex beads and bacteria were suspended at 0.01% (v/v) in DI water. An equal mixture of bacteria and beads in DI water was prepared immediately before the separation experiments to minimize aggregation. The conductivity of the DI water was measured to be 1 μS/cm. The latex particle polarizability, $\beta \cong -0.45-0.27i$ for 10–30 MHz, was calculated from the low-field measurements [11].

For testing devices, glass capillaries (285 μm outer diameter) were placed into the counterbores and epoxied in place. The capillary connections were then sealed with polydimethylsiloxane (GE RTV615A) to prevent leaking. Teflon tubing (30 gage) was run from the capillaries to a syringe and the fluid suspensions were injected manually. The dielectrophoretic gates were energized with a sinusoidal wave, 10 V peak-to-peak (pp) and 0.1–30 MHz, using a function generator. The experiments were recorded onto a videotape, and later digitized for analysis. The fluid velocities were estimated by calculating particle velocities on the videotape, either with the gates inactivated or when the particles were at large distances ($x > 50$ μm) from the activated gates.

Experimental Results

Figure 4(*a*) shows the separation of a mixture of 1 μm latex particles from dead Staphylococcus aureus bacteria. The gate was set to 10 v peak-to-peak at 15 MHz. It is evident that the positively polarized bacteria accumulate at the gate microelectrode, while the negatively polarized latex particles are repelled from the gate region. Upon injection of the mixture, the fluid velocity was measured to be 5–10 μm/s, and at this velocity, the latex particles formed a distinct front $\sim$40 μm upstream from the gate. In contrast, the bacteria accumulate at the gate, and, as the polarization interactions occur, long pearl chains of bacteria form that exceed the bounds of the gate. Three individual bacteria had their distance-dependent velocities, $u(x)$, tracked from their entrance into the channel until they came to rest at the tips of pearl chains 5 μm upstream from the gate (Fig. 4(*b*)). The fluid velocity was kept low (5–10 μm/s), which was much smaller than the DEP-induced particle velocity. The large DEP-induced particle velocities made it difficult to track bacteria within 20 μm of the gates, hence the velocity data were fitted to an exponential curve [$u = 1330e^{-0.122x}$ μm/s, x in micrometer, with $r^2 = 0.92$] to provide an estimate of the particle velocities generated near the gate. Thus, it was found that the bacteria were accelerated to velocities up to $\sim$700 μm/s before coming to rest adjacent to the gate. Using Eq. (3), the maximum estimated forces exerted on individual bacteria are on the order of 5 pN. Figure 4(*b*) also shows the velocity data of four latex particles that were tracked while undergoing nDEP. In addition, the fluid velocity was increased in order to examine the strength of the repulsive force. It was found that, after the latex particles were injected at velocities of 75–100 μm/s, the DEP force started to exert an observable deceleration of particles at $x \sim 30$ μm from the gate, with full repulsion bringing particles to a halt $\sim$12 μm upstream from the gate.

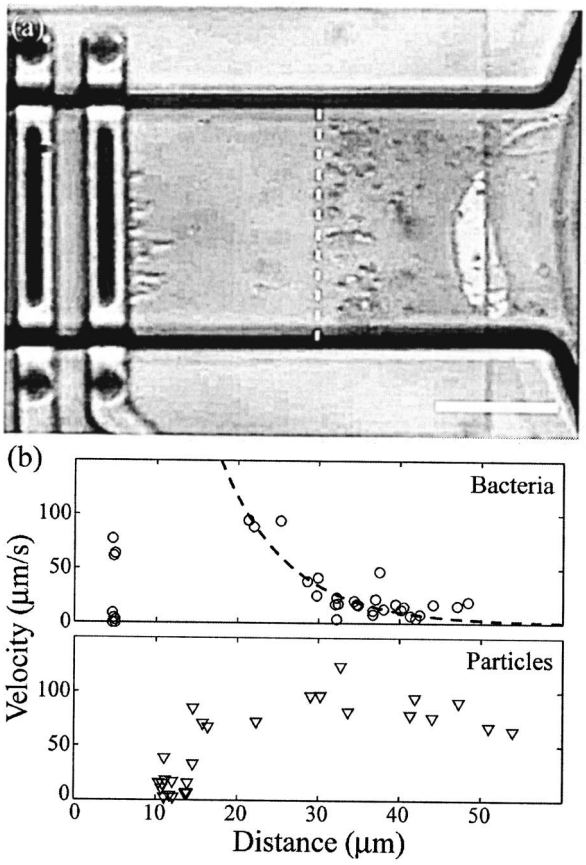

Fig. 4 (*a*) At 10 V pp, 15 MHz, bacteria adhere to the gate, while latex particles are repulsed and form a front (dashed line). Fluid velocity, 5–10 μm/s. Scale bar=20 μm. (*b*) DEP-induced velocity of bacteria (n=3) and latex particles (n=4) at 15 MHz as a function of distance from the center of the gate.

At higher fluid velocities, the latex particles formed fronts closer to the gate and the interparticle interactions became more apparent. In particular, at a fluid velocity of $\sim$45 μm/s (the flow rate $\sim$6 pL/s) the repelled latex particles aggregated at $x \sim 25$ μm upstream from the center of the gate with the average particle concentration in the aggregate running as high as 40–50% (v/v) (estimated from the images on the assumption that aggregates span the channel height) [11]. The particle aggregate oscillated between forming one bolus being located in the center of the channel and two rotating boluses being located at the channel sidewalls. Figure 5 documents that switching the gate frequency from 15 MHz to 100 kHz causes the particle aggregates adjacent to the channel sidewalls to traverse the gate, while the bacteria remain trapped, and in the presence of an estimated fluid velocity of 45 μm/s, all the accumulated latex particles escape the gate

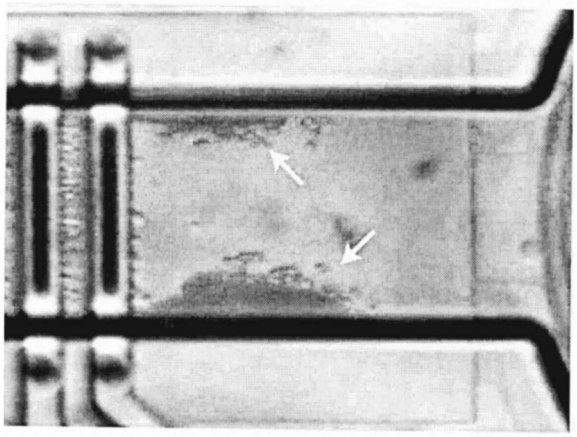

Fig. 5 Approximately 0.5 s after the frequency is switched from 15 MHz to 100 kHz, latex particles are traversing the gate along the sidewalls, while bacteria remain trapped. All accumulated latex particles escape the gate within 5 s following the frequency shift.

within ~5 s following this frequency shift. However, the pDEP force on the bacteria at this frequency is still strong enough to withstand the fluid flow. This release of the latex particles may be related to the reduction of their relative polarizability, $\mathrm{Re}(\beta^*)$, with decreasing field frequency, as was observed in [21] under similar conditions, or with an AC generated electroosmotic fluid flow caused by the action of the field along the double layer at the channel sidewalls [22]. Further analysis of the gate operation at submegahertz frequencies is in progress and will constitute the subject of future publication.

Discussion

Simulations of the profile of $\nabla \mathbf{E}^2_{\mathrm{rms}}$ provide a rough estimate for the DEP-induced velocity of individual bacteria and latex particles using Eq. (3). In particular, with $\nabla \mathbf{E}^2_{\mathrm{rms}} \sim 7 \times 10^{15}\ \mathrm{V}^2/\mathrm{m}^3$ at a distance of 20 μm from the center of the gate, the DEP-induced velocity of a single bacteria at this distance is estimated to be ~94–188 μm/s (estimating $\mathrm{Re}(\beta^*)$ to be in the range from 0.2 to 0.4), whereas the exponential fit of the experimental velocity data yields 108 μm/s. Measurements of $\mathrm{Re}(\beta^*)$ for the bacteria will be conducted in the future. The predictions of the DEP-induced velocity of the latex particles also agree with our observations in that, at a fluid velocity of 10 μm/s, a 0.5 μm radius latex particle should experience a drag force of ~0.08 pN if brought to rest by an opposing DEP force. Using our simulations for $\nabla \mathbf{E}^2_{\mathrm{rms}}$ and Eq. (1), $\mathbf{F}_{\mathrm{DEP}}$ should first reach 0.08 pN ~45 μm from the gate, which agrees reasonably with our observations of the formation of a particle front at 40 μm from the gate. At a fluid velocity of 45 μm/s, our simulations predict that the latex particles should be brought to rest at $x \sim 33$ μm upstream from the microelectrodes, while we observed the formation of a front at $x \sim 25$ μm from the gate. These estimates agree reasonably well with our observations. Several factors that have been neglected in these estimates are likely responsible for any discrepancies, for instance, interparticle interactions and additional hydrodynamic forces caused by the formation of particle aggregates in the channel.

The separation efficiency of the dielectrophoretic gate is optimal at relatively low fluid velocities and long separation times. No bacteria or particles were observed to escape the trap during its activation at 10 V, 15 MHz and at fluid velocities up to ~600 μm/s. Our simulations indicate that the gates should be able to repel particles traveling up to ~1000 μm/s. Latex particles were observed to traverse the gate only when the amount of collected particles began to fill the entire yz cross section of the channel in which case particles near the sidewalls, the weakest point of the $\mathbf{F}_{\mathrm{DEP}}$, were found to escape the gate.

Another phenomenon was observed in several instances when a bacterial cell adhered to a single latex particle thereby creating a bacteria-particle complex susceptible to pDEP which, therefore, was trapped at the gate. In such cases, within 5–10 s of the complex coming to rest, the latex particle was observed to break away from the bacteria and to accelerate toward the rest of the repelled particle aggregate upstream of the gate. Thus, longer separation times may be required to reduce the effect of this phenomenon, which could possibly contaminate the analysis and identification procedures conducted on the biosuspension.

Conclusions

We have described a surface-micromachined dielectrophoretic gate for separating micrometer-sized analytes based on their intrinsic polarizability properties and validated experimentally basic relations for estimating the gate performance. The separation technique uses AC dielectrophoresis along the flow streamlines accompanied by the field-induced phase separation through electrical and hydrodynamic interparticle interactions. The self-sealed microfluidic devices were fabricated using a surface- and bulk-micromachining technology, which is amendable to mass production. Setting the device to a moderate voltage in the radio frequency range selectively removed bacteria cells from a mixture containing nonbiological particles. The low aspect ratio of the device permitted a high-efficiency separation because the range of the dielectrophoretic force extended throughout the cross section of the fluid channel. This reduces the number of particles that escape the trap, producing highly concentrated (by factor over 500 the initial concentration) and spatially separated aggregates of negatively and positively polarizable analytes. We see a potential use for the proposed technology for discriminating between biological and nonbiological analytes that are captured in air samples. Future work is aimed at the optimization of the gating technique and the development of integrated biodetection systems.

Acknowledgment

The authors would like to thank Randy Shul and Peggy Clews of Sandia National Laboratories for their aid in the development of the DRIE counterbore microfluidic interconnect, and the development of the device release chemistry, respectively. We would also like to thank Larry Gilbert of Lockheed Martin for valuable discussions on biodetection. This work was supported, in part, by grants from the National Aeronautics and Space Administration, No. NAG3-2698 (B.K. and A.A.), the Defense Advanced Research Projects Agency (DARPA) through the Bioflips/Simbiosys Program, Mission Research Corporation/DARPA Contract No. DAAH01-02-C-R083 (B.K.), National Science Foundation, NSF-CTS-030799 (B.K. and A.A.), and the joint NSF/Sandia program (B.K.). D.B. thanks Sandia's MESA Institute and the NSF MAGNET/SEM program for support. Sandia is a multiprogram laboratory operated by Sandia Corporation, a Lockheed Martin Company, for the United States Department of Energy under Contract No. DE-ACO4-94-AL85000.

References

[1] (IOM) Institute of Medicine of the National Academies, Board on Health Sciences Policy, 1999, "Chemical and Biological Terrorism: Research and Development to Improve Civilian Medical Response," National Academy Press, Washington, DC, Chap. 6.

[2] TENG Solutions, 2002, "Protective Measures to Mitigate Chemical and Biological Threats for GSA Federal Buildings—Region 4," http://www.coa.gatech.edu/bc/research/, Georgia Institute of Technology, Atlanta GA.

[3] Chiem, N. H., and Harrison, D. J., 1998, "Microchip Systems for Immunoassay: An Integrated Immunoreactor With Electrophoretic Separation for Serum Theophylline Determination," Clin. Chem., **44**, pp. 591–598.

[4] Jiang, G., Attiya, S., Ocvirk, G., Lee, W. E., and Harrison, D. J., 2000, "Red Diode Laser Induced Fluorescence Detection With a Confocal Microscope on

a Microchip of Capillary Electrophoresis," Biosens. Bioelectron., **14**, pp. 861–869.
[5] Narang, U., Gauger, P. R., and Ligler, F. S., 1997, "A Displacement Flow Immunosensor for Explosive Detection Using Microcapillaries," Anal. Chem., **69**, pp. 2779–2785.
[6] Asami, K., 2002, "Characterization of Biological Cells by Dielectric Spectroscopy," J. Non-Cryst. Solids, **305**, pp. 268–277.
[7] Yang, L., Ruan, C., and Li, Y., 2003, "Detection of Viable *Salmonella Typhimurium* by Impedance Measurement of Electrode Capacitance and Medium Resistance," Biosens. Bioelectron., **19**, pp. 495–502.
[8] Gascoyne, P. R. C., Wang, X., Huang, Y., and Becker, F. F., 1997, "Dielectrophoretic Separation of Cancer Cells From Blood," IEEE Trans. Ind. Appl., **33**, pp. 670–678.
[9] Gascoyne, P. R. C., Satayavivad, J., and Ruchirawat, M., 2004, "Microfluidic Approaches to Malaria Detection," Acta Trop., **89**, pp. 357–369.
[10] Lapizco-Encinas, B. H., Simmons, B. A., Cummings, E. B., and Fintschenko, Y., 2004, "Insulator-Based Dielectrophoresis for the Selective Concentration and Separation of Live Bacteria in Water," Electrophoresis, **25**, pp. 1695–1704.
[11] Bennett, D. J., Khusid, B., Galambos, P. C., James, C. D., Okandan, M., Jacqmin, D., and Acrivos, A., 2003, "Field-Induced Dielectrophoresis and Phase Separation for Manipulating Particles in Microfluidics," Appl. Phys. Lett., **83**, pp. 4866–4868.
[12] Gascoyne, P. R. C., and Vykouval, J., 2002, "Particle Separation by Dielectrophoresis," Electrophoresis, **23**, pp. 1973–1983.
[13] Markarian, N., Yeksel, M., Khusid, B., Farmer, K., and Acrivos, A., 2003, "Particle Motions and Segregation in Dielectrophoretic Micro-Fluidics," J. Appl. Phys., **94**, pp. 4160–4169.
[14] Qiu, Z., Markarian, N., Khusid, B., and Acrivos, A., 2002, "Positive Dielectrophoresis and Heterogeneous Aggregation in High-Gradient AC Electric Fields," J. Appl. Phys., **92**, pp. 2829–2843.
[15] Dussaud, A. D., Khusid, B., and Acrivos, A., 2002, "Particle Segregation in Suspensions Subject to High-Gradient AC Electric Fields," J. Appl. Phys., **88**, pp. 5463–5473.
[16] Castellanos, A., Ramos, A., Gonzalez, A., Green, N. G., and Morgan, H., 2003, "Electrohydrodynamics and Dielectrophoresis in Microsystems: Scaling Laws," J. Phys. D, **36**, pp. 2584–2597.
[17] Halsey, T. C., 1992, "Electrorheological Fluids," Science, **258**, pp. 761–766.
[18] Kumar, A., Qiu, Z., Acrivos, A., Khusid, B., and Jacqmin, D., 2004, "Combined Negative Dielectrophoresis and Phase Separation in Nondilute Suspensions Subject to a High-Gradient AC Electric Field," Phys. Rev. E, **69**, 021402.
[19] Okandan, M., Galambos, P. C., Mani, S., and Jakubczak, J., 2001, "Development of Surface Micromachining Technologies for Microfluidics and BioMEMS," Proc. SPIE, **4560**, pp. 133–139.
[20] Laermer, F., and Schilp, A., 1996, "Method of Anisotropically Etching Silicon," U.S. Patent No. 5,501,893.
[21] Cui, L., Holmes, D., and Morgan, H., 2001, "The Dielectrophoretic Levitation and Separation of Latex Beads in Microchips," Electrophoresis, **22**, pp. 3893–3901.
[22] Ramos, A., Morgam, H., Green, N. G., and Castellanos, A., 1999, "AC Electric-Field-Induced Fluid Flow in Microelectrodes," J. Colloid Interface Sci., **217**, pp. 420–422.